

Tropospheric Planetary Wave Response to Anomalies in the Stratospheric Circulation

Grigory Nikulin¹ and François Lott

Laboratoire de Météorologie Dynamique, Ecole Normale Supérieure, Paris, France

Submitted to Journal of Climate

December 2007

¹Corresponding Address and Present affiliation:

Dr. Grigory Nikulin

Rossby Centre

Swedish Meteorological and Hydrological Institute

Folkborgsvägen 1

60176 Norrköping

Sweden

e-mail: grigory.nikulin@smhi.se

ABSTRACT

The NCEP-NCAR reanalysis is used to analyze the relationships between the state of the stratosphere and the tropospheric waves during the Northern Hemisphere (NH) winter. First, a cross-spectral analysis reveals that the strength of the polar vortex, measured by the 20-hPa Northern Annular Mode (NAM) index and the wave activity flux, measured by the vertical component of the Eliassen-Palm flux (EPz) from both the troposphere and the stratosphere, are significantly related with each other and in lead-lag quadrature at periods longer than 50-60 days only. The spectral analysis also shows that these periods are also those for which the downward propagation of stratospheric anomalies occurs, confirming that the downward propagation in the stratosphere is caused by wave-mean flow interaction at these low frequencies only. More specifically, we found that a weak (strong) polar stratospheric vortex is preceded by positive (negative) EPz anomalies and followed by negative (positive) EPz anomalies at all altitudes from the troposphere to the stratosphere.

We also found that at low frequencies, the EPz anomalies in the troposphere are significantly larger after stratospheric vortex anomalies than before. This marked difference in the troposphere is related to planetary waves with zonal wavenumbers 1-3, showing that there is a tropospheric planetary wave response to the earlier state of the stratosphere at low frequencies. We also find that this effect is eventually due to anomalies in the EPz issued from the northern midlatitudes and polar regions.

Most of these results are recovered using an entirely independent dataset, e. g. a 20-years integration done with the stratospheric version of the LMDz GCM. This validates the stratospheric planetary scale dynamics in the NH extratropics of this model and confirms that a stratosphere-troposphere connection occurs through the stratospheric variability driven by waves at periods longer than 50-60 days. However, even though the tropospheric EPz flux is

more pronounced after an anomaly in the stratospheric vortex than before the difference is not as strong as it is in the NCEP-NCAR reanalysis.

1. Introduction

In the Northern Hemisphere (NH) middle and polar latitudes, the stratospheric variability is very pronounced during the winter months. This follows from the fact that during this period, the stratospheric winds are eastward, which permits planetary waves to propagate into the stratosphere (Charney and Drazin 1961). The interaction between these waves and the large-scale flow can lead to very large changes in the mean stratospheric circulation. As planetary waves entering into the stratosphere have their origin in the troposphere, it seems reasonable to consider that the stratospheric variability is essentially a response to the tropospheric variability. This view is confirmed by the diagnostic studies in Newman et al. (2001) or Polvani and Waugh (2004) and which show that the anomalous state of the stratospheric polar vortex depends on the Wave Activity Flux (WAF) entering into the stratosphere from the troposphere during a preceding period.

In response to the waves coming from the troposphere, the stratosphere can develop its own modes of internal variability. Holton and Mass (1976) have shown that in a simplified model where the wave forcing is fixed at the lower boundary, the interaction between the planetary waves and the large-scale flow leads to nonlinear vacillations. This results were confirmed by Scott and Polvani (2006) using a General Circulation Model (GCM) of the stratosphere, where the tropospheric forcing is time-independent.

Over the last 10 years, a large number of studies have also suggested that an anomalously strong or weak stratospheric polar vortex influences the tropospheric circulation at a later stage. The low-frequency stratospheric anomalies, measured by the Arctic Oscillation (AO) index or by the zonal-mean zonal wind (\bar{u}), often propagate downward at the tropopause level, and sometimes deeper into the troposphere reaching the surface (Kodera et al. 1990; Baldwin and Dunkerton 1999; Christiansen 2001). Subsequent anomalies in the tropospheric circulation can be seen as long as several weeks after the initial stratospheric anomalies (Thompson et al. 2002, Polvani and Waugh 2004).

The low-frequency downward propagation in the stratosphere is also found in models of various complexity (Christiansen 2001; Plumb and Semeniuk 2003; Scott and Polvani 2004, Lott et al. 2005). These often show that the downward propagation in the stratosphere originates from local wave-mean flow interaction, somehow reminiscent of the dynamics the Quasi-Biennial Oscillation (QBO) in the tropical stratosphere. However, it is not clear if the downward propagation continuous from the tropopause to the ground, or if the downward propagation is the primary vector of the stratospheric influence on the troposphere. Among other mechanisms suggested are, (i) a remote response to stratospheric potential vorticity anomalies (Black 2002, Ambaum and Hoskins 2002), (ii) the downward control (Haynes 1991; Thompson et al. 2006), and (iii) the downward control with eddy feedback (Song and Robinson 2004).

Besides those “direct” effects on the troposphere, the stratospheric circulation can also affect eddy development in the troposphere at both synoptic and planetary scales. Upward propagating planetary waves can be reflected downward, hence modifying the planetary wave activity in the troposphere (Perlwitz and Harnik 2003). Recent model studies (Tanaka and Tokinaga 2002; Song and Robinson 2004; Wittman et al. 2004, 2007) have also shown that the baroclinic instability life cycle in the troposphere is sensitive to the state of the stratosphere, and in particular to the vertical shear of zonal wind (u_z) in the lower stratosphere. In this context, a stronger than usual polar night jet increases u_z near above the tropopause which can result in a modification of the planetary and synoptic baroclinic instability. Topographically forced quasi-stationary planetary waves in the troposphere are also sensitive to the stratospheric conditions, so they can also respond to downward propagating stratospheric anomalies in zonal-mean zonal wind \bar{u} (Coughlin and Tung 2005).

The fact that there is a stratospheric influence on the tropospheric waves is also apparent in Karpetchko and Nikulin (2004) who found that in situations where the January-February polar night jet is stronger than usual there is an enhanced equatorward wave refraction (see also

Hartmann et al. 2000), and that there is also an increase of the upward WAF in both the troposphere and the stratosphere. Nevertheless, the main results in Karpetchko and Nikulin (2004) are based on the fact that the upward WAF at 20 hPa averaged for the early winter (November-December), is anticorrelated with the upward WAF averaged for midwinter (January-February). They mentioned that this anticorrelation is associated with changes in the lower stratospheric circulation in midwinter but they did not examine if the changes in the stratospheric circulation can result in changes in the WAF at a later stage.

The main purpose of this paper is to clarify these last results, namely that there is a low-frequency relationship between the stratospheric circulation and the tropospheric waves at a latter stage. As the variability in the stratosphere is dominated by the Northern Annular Mode (NAM), which anomalies are themselves driven by the WAF anomalies, we will follow Karpetchko and Nikulin (2004) and establish our results using these two diagnostics. Nevertheless, and before addressing this issue specifically, we will first clarify at which time scales the stratospheric circulation affects the surface climate. This aspect needs a careful attention because in the past, the downward propagation has been identified using a large variety of ad-hoc low-pass filters: a one month averaging is used in Kodera et al. (1990), a two month averaging in Karpetchko and Nikulin (2004), a 90-day low-pass filter in Baldwin and Dunkerton (1991) and a 30-350 day bandpass filter in Christiansen (2001). There is clearly a need for a more systematic identification of the frequency domain over which the downward propagation occurs. It also important to design filters which minimize the Gibbs effects and the overshoots/ringings in the filtered fields: all these can yield to spurious oscillatory behaviors.

The plan of the paper is as follows. Section 2 presents the datasets and the methods. The characteristic time scales for the downward propagation and for the coupling between the NAM index and the upward WAF at different levels are analyzed by a cross-spectral analysis in section 3. Section 4 describes the difference between preceding and subsequent wave

forcing about extremes in the strength of the stratospheric polar vortex. The analysis in Section 4 focuses on the low-frequency intraseasonal band revealed by the spectral analysis in section 3, and using a low-pass filter appropriate for this frequency band. Our main results are summarized in Section 5. Some discussions about the origin of the stratosphere-troposphere couplings established in this paper are also given in Section 5.

2. Data and method

The first database we use is the daily NCEP-NCAR reanalysis for the 1978-2005 period (Kalnay et al. 1996). To verify that the results obtained do not depend on the database chosen, we have also used the daily ERA-40 reanalysis for the 1978-2002 period (Uppala et al. 2005). Since the results are identical, the results from the NCEP-NCAR reanalysis are only presented here. Finally, we also perform the same analysis on the stratospheric version of the LMDz General Circulation Model presented in Lott et al. (2005). For completeness note that the LMDz GCM is a gridpoint model in the horizontal direction with a uniform resolution of 2.5° in latitude and 3.75° in longitude. The vertical resolution is in term of a hybrid sigma-pressure vertical coordinate with an upper boundary at near 65 km. The model results presented are from a 20 year integration forced at the lower boundary by sea surface temperature and sea ice cover that vary along a climatological annual cycle.

For all datasets, the daily anomalies are calculated by subtracting the daily climatological annual cycle. The variability of the zonal mean state is characterized by the NAM pattern defined at each level as the leading empirical orthogonal function (EOF) of the monthly-mean zonal-mean geopotential height anomalies north of 20°N . The daily NAM index is then constructed by projecting daily zonal-mean geopotential height anomalies onto the leading EOF pattern. A positive value of the NAM index in the stratosphere corresponds to a stronger than usual polar night jet. The vertical component of the quasigeostrophic Eliassen-Palm (EP) flux in spherical coordinates $F^{(z)}$ is used as a measure of the vertical wave activity flux

(Edmon et al. 1980; Andrews et al. 1987). As an integral measure of wave forcing for the NH we use the vertical EP flux averaged over the 45°-75°N,

$$\langle F^{(z)} \rangle = \int_{45}^{75} F^{(z)} \cos \varphi d\varphi, \quad (1)$$

where φ is the latitude.

To focus attention on the variability of the atmosphere in specific frequency bands, we apply a finite impulse response filter based on the sinc function. The filter Kernel h_f is given by

$$h_f(i) = \frac{\sin(2\pi fi)}{2\pi fi}, \quad -N \leq i \leq N, \quad (2)$$

where f is the cutoff frequency (or the half power point in the spectral domain), and where $2N+1$ is the filter length (Smith 2002). The filter length is chosen equal to the cutoff period in days. This is an optimal choice, yielding to a rather sharp transition in the frequency domain near f but resulting in small overshoots and ringings in the step response. To minimize the Gibbs effect the filter kernel is multiplied by a Kaiser window with a sidelobe attenuation of 50 dB (Thede 2004).

To determine the frequency band at which the NAM index and the vertical EP flux are related with each other, we compute the coherence and phase spectra between them. To evaluate these spectral estimates we first focus onto the NH winter period and divide the data into non-overlapping samples of equal length (365 days) beginning at 1 July and ending at 30 June next year. Each sample is detrended and a cosine bell taper is applied to the first and last 90 points. For each sample of the NAM and the vertical EP flux we take the Fourier transform and evaluate the individual periodograms and cross-periodograms. The spectral and cross-spectral estimates for calculation of the coherence and phase spectra are then obtained by averaging the individual periodograms and cross-periodograms.

The statistical significance for the coherence spectra are determined by a Monte-Carlo method. The Monte-Carlo test uses 500 pair of an autoregressive process of order 1 (AR1) with variance and lag 1 autocorrelation estimated from the original data. In each pair, the AR1 surrogates are independent of each other, hence, the test for the coherency spectrum evaluates in which frequency band the original series are significantly related. For each surrogate pair the coherency spectrum is estimated exactly as it is for the original series. For each frequency, this yields to 500 estimates of the coherency between two unrelated AR1 processes, and from these 500 values we collect statistics for the 95% and 99% confidence levels. Although this method does not take into account the fact that in the original data most of the variability occurs during the winter season we have verified that weighting the artificial time series by an annual cycle for the variance affect little our test (see also Christiansen 2001).

Since there is no method to derive the statistical significance for the phase spectrum from the artificial time series we compute the confidence intervals for the phase spectra based on the t statistics (e. g. von Storch and Zwiers 1999, p. 285). Dividing the original data into 27 samples (NCEP-NCAR) gives approximately 54 degrees of freedom for the phase spectrum estimates.

We use similar method as for coherence to compute cross correlations between the filtered time series. First, a filter is applied to the original data, and then the filtered data is divided into non-overlapping “winter” samples beginning at October 1 and ending at April 30 next year. Each sample is detrended, individual cross correlations are calculated and averaged. The same sequence is used to estimate the 5% and 1% significance levels for the cross correlations by the Monte-Carlo test, from 500 pair of low-pass filtered AR1 surrogates independent of each other.

3. NAM-EP flux coupling and downward propagation

To determine the time scales on which the stratospheric NAM variability is related to the EP flux variability, Figure 1 presents the coherence and phase spectra between the NAM at 20 hPa and the vertical component of the EP flux at 100 and 500 hPa averaged over 45°-75°N (e.g. $\langle F^{(z)} \rangle$). For the NCEP-NCAR reanalysis, the coherence between the 20-hPa NAM index and the 100-hPa $\langle F^{(z)} \rangle$ is significant for all periods longer than 5 days (Fig. 1a) and substantially increases when the period increases. The corresponding phase (Fig 1b) is positive and close to 90°. Rather similar results are found when $\langle F^{(z)} \rangle$ is taken at other levels in the lower stratosphere but above 100 hPa (not shown). When the averaged vertical EP flux $\langle F^{(z)} \rangle$ is evaluated below 100 hPa, the coherence decreases, but remains significant in several frequency bands, including the low-frequency band at periods longer than 50 days (see for instance Fig. 1c). The phase at low frequencies is positive and significantly different from zero in both the stratosphere (Fig. 1b) and the troposphere (Fig 1d) with $\langle F^{(z)} \rangle$ is almost in lead-lag quadrature with the NAM index. This lead-lag quadrature indicates causality but does not tell who precedes the other. It can be due to that the $\langle F^{(z)} \rangle$ anomalies lead the NAM anomalies of the opposite sign and/or to that the $\langle F^{(z)} \rangle$ anomalies follow the NAM anomalies of the same sign. The fact that vertical EP flux anomalies lead the stratospheric NAM anomalies of the opposite sign is in agreement with previous findings of Newman et al. (2001) and Polvani and Waugh (2004), who showed that negative anomalies in wave forcing precede positive anomalies in the strength of the polar vortex and vice versa.

The coupling at low frequencies in Fig. 1 is probably an integral part of the dynamics of the low-frequency downward propagation of stratospheric anomalies documented by various authors (Kodera et al. 1990; Baldwin and Dunkerton 1999; Christiansen 2001), and providing that the time scales correspond. To establish this more precisely we next proceed to a cross-spectral analysis between the NAM indices at 10 and 70 hPa. These two levels are chosen

here for convenience, and because the signature of the downward propagation clearly appears between them.

Similarly to the coherence between the NAM index at 20 hPa and the EP flux at 100 hPa in Fig. 1a, the coherence between the NAM indices at 10 and at 70 hPa in Fig. 2a increases when the frequency decreases. According to the phase spectrum in Fig. 2b the coherence spectrum can be separated into two frequency bands. The first one is at periods longer than 50-60 days where the phase is positive thus the signal at 10 hPa leads the signal at 70 hPa indicating downward propagation. A cross-correlation analysis of the 60-day low-passed NAM index (not shown) reveals that the downward propagation of the NAM signal from 10 hPa into the lower stratosphere takes about 10 days and then a weak signal appears near the ground. The second band is approximately between 10 and 50 days where the phase has a tendency to be negative but the value is hardly different from zero. The main point here is that the downward propagation of the stratospheric anomalies into the lower stratosphere occurs in the low-frequency band at periods longer than 50-60 days where the coherence between the 20-hPa NAM index and $\langle F^{(z)} \rangle$ is found in both the stratosphere and the troposphere (see Fig. 1). The same characteristic time scales of the downward propagation and the high coherence between the NAM and $\langle F^{(z)} \rangle$ in the stratosphere support the previous observational and model studies (Christiansen 2001; Plumb and Semeniuk 2003) suggesting that the downward propagation in the stratosphere is driven by low-frequency wave forcing through local wave-mean flow interaction.

The cross-spectral analysis applied to the 20-year simulation with the LMDz GCM (not shown) gives results which are almost identical to the one applied to the NCEP-NCAR reanalysis. The model reproduces well the lead-lag quadrature and coherence between the 20-hPa NAM and $\langle F^{(z)} \rangle$ in both the stratosphere and the troposphere at periods longer than 50-60 days, as well as the downward propagation at the same periods. Hence the low-frequency

stratospheric behavior and the downward propagation in the LMDz GCM are essentially a response to the low-frequency variability of the wave forcing, as in the observations.

4. NAM: preceding and subsequent wave forcing

4.1. December-January NAM

To identify at which latitudes and altitudes the low-frequency lead-lag relationships between the NAM index at 20 hPa and the vertical EP flux $F^{(z)}$ are more pronounced, we partly follow Karpetchko and Nikulin (2004) and differentiate $F^{(z)}$ averaged for November-December (ND) to $F^{(z)}$ averaged for January-February (JF) according to the 20-hPa NAM index averaged for December-January (DJ). For these purposes, the Figs. 3a, b show the one point correlations of the DJ NAM index at 20 hPa with the ND $F^{(z)}$ and the Figs. 3c, d show the one point correlations of the DJ NAM index at 20 hPa with the JF $F^{(z)}$. The averaging period for the NAM index is centered about the averaging periods for $F^{(z)}$ and partly overlaps them implying that the ND $F^{(z)}$ precedes the DJ NAM index and the JF $F^{(z)}$ follows the DJ NAM index. For the preceding period and for the NCEP-NCAR reanalysis, we find a strong negative correlation in the stratosphere (Fig. 3a), in agreement with Newman et al. (2001) and Polvani and Waugh (2004). This result is consistent with the fact that strong (weak) $F^{(z)}$ precedes a weak (strong) polar vortex. In contrast, for the subsequent period and still for the NCEP-NCAR reanalysis (Fig. 3c), there is a positive correlation indicating that a strong (weak) $F^{(z)}$ follows a strong (weak) polar vortex. We should note that the correlation pattern in Fig. 3c is almost identical to the one obtained in Karpetchko and Nikulin (2004), where the correlation between the ND eddy heat flux at 20 hPa (45°-75°N) and the JF eddy heat flux is shown (see their Fig. 1a). Our results here thus prove that the anticorrelation between the early winter wave forcing and the midwinter wave forcing found by these authors is associated with anomalies in the stratospheric NAM.

If we now return to Figs 3a and 3c, we can see that there is a noticeable difference in the lat-altitude distribution of the vertical EP flux that produces the changes in the NAM at 20 hPa. For instance, in the stratosphere, the ND $F^{(z)}$ is anticorrelated with the 20-hPa NAM over a large domain (50°-80°N) corresponding to the stratospheric jet. On the contrary, and still in the stratosphere, the JF $F^{(z)}$ is significantly correlated with the 20-hPa NAM over a much narrower domain. If we assume that the lower stratosphere is more disturbed after 20-hPa NAM anomalies than before (and because this anomaly propagates downward interacting with planetary waves), this difference in pattern between the ND $F^{(z)}$ and the JF $F^{(z)}$ correlations can be viewed as a signature of the downward propagation of the NAM signal.

A more significant signal is found in Fig. 3c in the troposphere between 60° and 80°N. It shows that there is a strong tropospheric EP flux anomaly occurring after a NAM event. It is much stronger and broader in latitude than the opposite signal found in the troposphere in early winter (see Fig. 3a). As again, the middle and lower stratosphere is much more disturbed after a 20-hPa NAM event, this difference is our first evidence that the stratospheric circulation affects the tropospheric waves at a later stage.

The same one-point correlations for the LMDz GCM are shown in Figs. 3b, d (right). Two main results found in the observations are also present in the model: the negative correlations in ND (Fig. 3b) and the positive correlations in JF (Fig. 3d). The LMDz GCM also reproduces that in ND the negative correlation in the extratropical stratosphere (Fig 3b) is stronger in amplitude than the opposing positive correlation found in JF (Fig. 3d). Note also, that in the LMDz GCM, there is a strong tropospheric correlation in midwinter (JF, Fig. 3d) which has no opposing counterpart in early winter (ND, Fig. 3b). Although less pronounced than in the reanalysis, this difference in the troposphere witnesses again that there is a dynamical influence of the stratosphere on the tropospheric waves.

Finally, and to determine which waves are responsible for the $F^{(z)}$ correlation in Fig. 3, we have partitioned the total $F^{(z)}$ into $F^{(z)}$ due to the zonal waves 1-3 and that due to the waves

4-7. This partitioning shows that the waves 1-3 are the main contributor to the observed correlation patterns at least north of 45°N for both the reanalysis and the LMDz GCM. Only the negative correlation in the subtropical lower stratosphere for JF (Figs. 3c and 3d) is related to the waves 4-7.

4.2. *Daily low-passed NAM*

The two-month boxcar average used in Fig. 3 is equivalent to applying a low-pass filter with half-power point at 100 days. It therefore excludes a good part of the coherence seen in Fig. 1 and which occurs for all periods longer than 10 days. It also excludes a part of the downward propagating NAM signal which starts to propagate downward at periodicities longer than 50 days (see the thin vertical line in Fig. 2b). To capture both effects more completely, and also to select other months for the NAM than JF only, we next filter all our daily series with the 60-day low-pass filter given in Eq. 2.

The Fig. 4 shows the cross correlation of the daily NAM index at 20 hPa with itself (thick lines in the top panels) and with the daily vertical EP flux averaged over 45°-75°N ($\langle F^{(z)} \rangle$). Again, the reanalysis (top panels in Fig. 4) and the LMDz GCM (bottom panels in Fig. 4) are in good agreement with each other. The typical duration of the low-frequency NAM events is approximately two months, and the difference in sign for the $\langle F^{(z)} \rangle$ anomalies between subsequent and preceding periods found in Fig.3, is even clearer now. In the stratosphere the strongest negative correlations are observed when the EP flux $\langle F^{(z)} \rangle$ leads the NAM index by about 20 days, while the strongest positive correlations are found when $\langle F^{(z)} \rangle$ follows the NAM index by about 25 days. In the troposphere, the correlations in Fig.4 are in general weaker than the stratospheric ones, but the values are still significant at both positive and negative lags. Note nevertheless, that the tropospheric correlations at positive lags are much larger in amplitude than those at negative lags, which was not the case in the stratosphere. The

cross-correlation patterns in Fig. 4 are also consistent with the phase spectra in Fig. 1, where the NAM and $\langle F^{(z)} \rangle$ at low frequencies are close to lead-lag quadrature: the extremes in the $\langle F^{(z)} \rangle$ anomalies (forcing) almost coincide with zero values of the NAM anomalies (response) and zero values for $\langle F^{(z)} \rangle$ are at near zero lag with respect to the NAM extremes.

At first sight, the positive correlations in Fig. 4 and at positive lags could be interpreted as a negative feedback between the NAM index and $\langle F^{(z)} \rangle$ at a later stage. Nevertheless, for low-pass filtered series, it is mandatory to recall that such a phase relationship is always present when a forcing drives a change even in the absence of feedback of the change on the forcing. What is more meaningful in this context, is that—in the troposphere, the positive correlations at positive lags are much larger in amplitude than the negative correlations found at negative lags. This marked asymmetry in the troposphere, with a more pronounced signal at positive lag, can not be reproduced by a simple statistical model where one series forces the changes in the other without feedback. Accordingly, and providing that this difference in amplitude is significant (see the end of this section), we will interpret it as a feedback of the stratospheric state on the tropospheric wave activity flux. Note that a similar contrast in the troposphere was shown in Fig. 3 for the two months averaging. The difference is more pronounced for the reanalysis throughout the troposphere than for the LMDz GCM, where the difference is weaker and essentially confined to the lower troposphere.

To determine the spatial distribution of the wave response, the Fig. 5 presents the cross correlation of the 20-hPa NAM with $F^{(z)}$ rather than with the latitude average of this quantity (e.g., $\langle F^{(z)} \rangle$) as was done in Fig. 4). For the NCEP-NCAR reanalysis, and in agreement with the results in Fig. 4, the correlations are about maxima in the stratosphere at lags -25 days (Fig. 5a) and 25 days (Fig. 5d). In the stratosphere, the maximum amplitude of the correlation at negative lag is around 0.6, it is almost equal to the maximum amplitude of the positive correlation at positive lag. This follows that $F^{(z)}$ causes the NAM variability, e. g. its onset

(negative lag) as well as its decay (positive lag). Accordingly the large positive correlation at positive lag in the stratosphere is not an indication of that the NAM itself influences $F^{(z)}$. In the stratosphere such an effect is more evident in the negative value for $F^{(z)}$ in the subtropics at positive lag (Figs. 5c, d), and which has no positive counterpart at negative lag. On the contrary, the Fig. 5 indicates that the correlation in the troposphere at positive lag is very pronounced in the polar latitudes where the tropospheric correlation at negative lag is much smaller in amplitude (see for instance Fig. 5a). The first sign of this tropospheric signal appears near lag -10 days north of 70°N (Fig. 5b). This signal extends equatorward reaching the maximum at lag 10 days near 400 hPa and 70°N (Fig. 5c). As for the results for the two month averaging, it is the waves with zonal wavenumber 1-3 that contribute to the cross-correlation patterns based on the low-passed daily data in Figs. 4 and 5 (not shown).

The same analysis for the LMDz GCM (not shown) also reveals a positive and significant tropospheric signal in $F^{(z)}$ after a NAM event, centered around 60°N. It is also larger in amplitude than the negative tropospheric signal seen before. Nevertheless, the difference in amplitude between the $F^{(z)}$ anomalies occurring after and before NAM events is not as pronounced as it is in the reanalysis dataset. As for the reanalysis the tropospheric signals in the LMDz GCM are associated with the planetary waves 1-3.

As said above, the presence of significant values in the cross correlation between the NAM and the vertical EP flux $F^{(z)}$ at positive lag in Figs. 4 and 5, is not an indication that the NAM affects the EP flux in return. It is more the differences in amplitude between the values at positive lags and those at negative lags that are meaningful in this respect. To test that these differences are significant, we next consider again the cross-correlations between the 20-hPa NAM and the vertical EP flux over 45°-75°N $\langle F^{(z)} \rangle$. We choose to test the cross correlation in the stratosphere at 100 hPa and, in the troposphere at 400 hPa. We also include in the test, cross correlation between the 20-hPa NAM and the EP flux $F^{(z)}$ at one point (400 hPa, 70°N)

where the strongest positive cross correlations are found in Fig. 5c. For the cross correlations chosen (see Fig. 6), we identify the positive lag for which the correlation is maximum and the negative lag for which it is minimum. We then take correlations at these negative (r_{\min}) and positive (r_{\max}) lags for each year. Two samples \mathbf{R}_{\min} and \mathbf{R}_{\max} are not independent each of other, since positive correlation follows negative correlation during the NAM life cycle, so we apply a one-side paired difference permutation test. We evaluate the difference between the absolute values of the two correlations $\mathbf{D}=|\mathbf{R}_{\max}|-|\mathbf{R}_{\min}|$, and the null hypothesis is that the mean of the difference - $\bar{\mathbf{D}}$ is equal or less than zero ($H_0 : \bar{\mathbf{D}} \leq 0$). For the permutation test we take absolute values of the difference $|\mathbf{D}|$, then randomly assign signs to $|\mathbf{D}|$ and compute the mean of randomly signed $|\mathbf{D}|$. The p -values are estimated from the resulting resampling distribution based on 500 permutations.

The estimated p -values in Table 1 give a strong evidence that for the NCEP-NCAR reanalysis the tropospheric EP flux anomalies are significantly larger in amplitude after a NAM event than before, especially in the polar region. At the same time there is no evidence that an increase in the tropospheric EP flux caused by the stratospheric circulation is felt in the stratosphere. The same test applied to the LMDz GCM results shows that the difference between positive and negative lags is less significant in the troposphere. The most significant result is for the correlation between the 20-hPa NAM and the 500-hPa $\langle F^{(z)} \rangle$, where the difference between the maximum correlation at positive lag and the minimum correlation at negative lag, is significant at the 15% level (not shown).

5. Conclusion

5.1. Summary

Various pieces of observational evidence are given to show that in the low-frequency band, an anomalous state of the stratosphere modulates the tropospheric planetary wave signal. The stratospheric NAM index approximating the variability of the zonal mean state and the

vertical EP flux anomalies from the stratosphere and the troposphere are significantly related with each other, at periods longer than 50-60 days. At these periods, the EP flux and the NAM are almost in lead-lag quadrature: the low-frequency EP flux anomalies of opposite sign about NAM events drive the onset and the subsequent decay of NAM events. It is found that the downward propagation of stratospheric anomalies also occurs in the same low-frequency band, e. g. at periods longer than 50-60 days. This coincidence of characteristic time scales for the downward propagation and for the high coherence between the NAM and the EP flux in the stratosphere clearly shows that the downward propagation in the stratosphere is the result of wave-mean flow interaction at low frequencies.

There is also a remarkable effect in the troposphere and in the same low-frequency band. The tropospheric EP flux anomalies coherent with the stratospheric NAM index are stronger in amplitude more than a week after a NAM event than at any time before. In this context, at periods longer than 50-60 days, a stronger (weaker) polar vortex leads to a subsequent increase (decrease) in the upward EP flux in the troposphere. At the same time there is no evidence of a corresponding increase in the upward EP flux in the stratosphere. The response of the tropospheric upward EP flux to the stratospheric conditions is related to waves with zonal wavenumbers 1-3, witnessing that there is a stratospheric influence on the low-frequency planetary waves in the troposphere. It is also important to recall that these results has been found using two entirely independent datasets, the NCEP-NCAR reanalysis dataset and the stratospheric version of the LMDz GCM (Lott et al. 2005)

5.2. *Discussion*

In the past, at least two dynamical mechanisms have been proposed to explain the planetary-scale tropospheric wave response to the state of the stratosphere.

The first mechanism is the modulation of the quasi-stationary planetary waves by the zonal mean state. It is related to the fact that in the troposphere, the amplitude of quasi-

stationary planetary waves is a function of the amplitude of the zonal wind \bar{u} and that even a small change in \bar{u} , can lead to large changes in the amplitude of the quasi-stationary waves (Branstator 1984; Nigam and Lindzen 1989; Kang 1990; Ting et al. 1996, DeWeaver and Nigam 2000). In this framework, stronger than usual \bar{u} causes an increase in the amplitude of the quasi-stationary waves. Providing that the downward propagation also influences the tropospheric \bar{u} anomalies (see Kodera et al. 1990 or Christiansen 2001 where this is established by other means), we can expect this to be at work in our cases as well. This point is illustrated using in Fig. 7a which presents a cross correlation between the 60-day low-passed 20-hPa NAM index and the \bar{u} anomalies at lag 10 days, e. g. when the maximum of the cross correlations between the NAM and the EP flux was found in the polar troposphere (see Fig. 5c). Although there is no coherence in the middle and upper polar troposphere, a significant coherence is evident in the lower troposphere north of 50°N. As the modulation of the planetary wave forcing is in good part controlled by the low-level winds (Held and Ting 1990) the Fig. 7a is consistent with the picture that stratospheric changes can affect, at a later stage, the tropospheric quasi-stationary wave forcing.

The second mechanism is related to the fact that the planetary-scale baroclinic instability in the troposphere are modulated by changes in the lower stratospheric vertical wind shear \bar{u}_z . Wittman et al. (2007), for instance, have shown that an increased \bar{u}_z in the lower stratosphere increases the growth rates of baroclinic modes with synoptic wavenumbers 4-7. At the same time, the planetary-scale modes of baroclinic instability can also be more unstable although they grow more slowly than the synoptic ones (Tanaka and Tokinaga 2002). If we recall that during winter, the wave-driven low-frequency anomalies in the lower stratosphere have long persistence (Baldwin et al. 2003) and can potentially influence baroclinic instability growing on timescales near a month, this mechanism can also be at work to explain our results. To check that it is indeed the case, the Fig. 7b shows that at periods longer than 60 days, the stratospheric \bar{u}_z anomalies are strongly correlated with the 20-hPa

NAM index, and that the signal even penetrates into the upper troposphere. This result is also coherent with recent model studies which demonstrate that high-latitude planetary wave baroclinic instabilities are more unstable when the polar vortex is stronger (Tanaka and Tokinaga 2002; Song and Robinson 2004). One more point in our results which is also consistent with the model result in Tanaka and Tokinaga (2002) or Song and Robinson (2004) is that the tropospheric planetary wave response we identify is essentially confined to the polar troposphere (Figs. 5b and 5c here).

Acknowledgments

The authors thank the Climate Prediction Center for providing the NCEP-NCAR reanalysis data and ECMWF for providing the ERA-40 reanalysis.

References

- Ambaum, H. P., and B. J. Hoskins, 2002: The NAO troposphere–stratosphere connection. *J. Climate*, **15**, 1969-1978.
- Andrews, D. G., J. R., Holton, and C. B. Leovy, 1987: *Middle Atmosphere Dynamics*. Academic Press, 489 pp.
- Baldwin, M. P., and T. J. Dunkerton, 1999: Propagation of the Arctic Oscillation from the stratosphere to the troposphere. *J. Geophys. Res.*, **104**, 30 937-30 946.
- Baldwin, M. P., D. B. Stephenson, D. W. J. Thompson, T. J. Dunkerton, A. J. Charlton, and A. O'Neill, 2003: Stratospheric memory and skill of extended-range weather forecasts. *Science*, **301**, 636-640.
- Black, R. X., 2002: Stratospheric forcing of surface climate in the Arctic oscillation. *J. Climate*, **15**, 268-277.
- Branstator, G., 1984: The relationship between zonal mean flow and quasi-stationary waves in the midtroposphere. *J. Atmos. Sci.*, **41**, 2163-2178.
- Charney, J. G., and P. G. Drazin, 1961: Propagation of planetary-scale disturbances from the lower into the upper atmosphere. *J. Geophys. Res.*, **66**, 83-109.
- Christiansen, B., 2001: Downward propagation of zonal mean zonal wind anomalies from the stratosphere to the troposphere: Model and reanalysis. *J. Geophys. Res.*, **106**, 27 307-27 322.
- Coughlin, K., and K. K. Tung, 2005: Tropospheric wave response to decelerated stratosphere seen as downward propagation in northern annual mode. *J. Geophys. Res.*, **110**, D01103, doi: 10.1029/2004JD004661.
- DeWeaver, E., and S. Nigam, 2000: Zonal-eddy dynamics of the North Atlantic oscillation. *J. Climate*, **13**, 3893-3914.
- Edmon, H. J., B. J. Hoskins, and M. E. McIntyre, 1980: Eliassen- Palm cross section for the troposphere. *J. Atmos. Sci.*, **37**, 2600-2616.

- Hartmann, D. L., J. M. Wallace, V. Limpasuvan, D. W. J. Thompson, and J. R. Holton, 2000: Can ozone depletion and global warming interact to produce rapid climate change? *Proc. Natl. Acad. Sci.*, **97**, 1412-1417.
- Haynes, P. H., M. E. McIntyre, T. G. Shepherd, C. J. Mark, and K. P. Shine, 1991: On the “downward control” of extratropical circulation by eddy-induced mean zonal forces. *J. Atmos. Sci.*, **48**, 651-680.
- Held, I. M., and M. Ting, 1990: Orographic versus thermal forcing of stationary waves: the importance of the mean low-level wind. *J. Atmos. Sci.*, **47**, 495-500.
- Holton, J. R., and C. Mass, 1976: Stratospheric vacillation cycles. *J. Atmos. Sci.*, **33**, 2218-2225.
- Kalnay, E., and Coauthors, 1996: The NCEP/NCAR 40-year reanalysis project. *Bull. Amer. Meteor. Soc.*, **77**, 437-471.
- Kang, I.-S., 1990: Influence of zonal mean flow change on stationary wave fluctuations. *J. Atmos. Sci.*, **47**, 141-147.
- Karpetchko, A., and G. Nikulin, 2004: Influence of early winter upward wave activity flux on midwinter circulation in the stratosphere and troposphere. *J. Climate*, **17**, 4443-4452.
- Kodera, K., K. Yamazaki, M. Chiba and K. Shibata, 1990: Downward propagation of upper stratospheric mean zonal wind perturbation to the troposphere. *Geophys. Res. Lett.*, **17**, 1263-1266.
- Lott, F., L. Fairhead, F. Hourdin, and P. Levan, 2005: The stratospheric version of LMDz: dynamical climatologies, arctic oscillation, and impact on the surface climate. *Climate Dyn.* **25**, 851-868, doi: 10.1007/s00382-005-0064-x.
- Newman, P. A., E. R. Nash, and J. E. Rosenfield, 2001: What controls the temperature of the Arctic stratosphere during the spring? *J. Geophys. Res.*, **106**, 19 999-20 010.
- Nigam, S., and R. S. Lindzen, 1989: The sensitivity of stationary waves to variations in the basic state zonal flow. *J. Atmos. Sci.*, **46**, 1746-1768.

- Perlwitz, J., and N. Harnik, 2003: Observational evidence of a stratospheric influence on the troposphere by planetary wave reflection. *J. Climate*, **16**, 3011-3026.
- Plumb, R. A., and K. Semeniuk, 2003: Downward migration of extratropical zonal wind anomalies. *J. Geophys. Res.*, **108**, 4223, doi:10.1029/2002JD002773.
- Polvani, L. M., and D. W. Waugh, 2004: Upward wave activity flux as precursor to extreme stratospheric events and subsequent anomalous surface weather regimes. *J. Climate*, **17**, 3548-3554.
- Scott, R. K., and L. M. Polvani, 2004: Stratospheric control of upward wave flux near the tropopause. *Geophys. Res. Lett.*, **31**, L02115, doi:10.1029/2003GL017965.
- Scott, R. K., and L. M. Polvani, 2006: Internal variability of the stratosphere. Part I: Time-independent forcing. *J. Atmos. Sci.*, **63**, 2758-2776.
- Smith, S., 1997: *Digital Signal Processing: A Practical Guide for Engineers and Scientists*. Newnes, 672 pp.
- Song, Y., and W. A. Robinson, 2004: Dynamical mechanism for stratospheric influence on the troposphere. *J. Atmos. Sci.*, **61**, 1711-1725.
- Tanaka, H. L., and H. Tokinaga, 2002: Baroclinic instability in high latitudes induced by polar vortex: a connection to the Arctic oscillation. *J. Atmos. Sci.*, **59**, 69-82.
- Thede, L., 2004: *Practical Analog And Digital Filter Design*. Artech House, 270 pp.
- Thompson, D. W. J., M. P. Baldwin, and J. M. Wallace, 2002: Stratospheric connection to Northern hemisphere wintertime weather: implications for prediction. *J. Climate*, **15**, 1421-1428.
- Thompson, D. W. J., J. C. Furtado, and T. J. Shepherd, 2006: On the tropospheric response to anomalous stratospheric wave drag and radiative heating. *J. Atmos. Sci.*, **63**, 2616-2629.
- Ting, M., M. P. Hoerling, T. Xu, and A. Kumar, 1996: Northern Hemisphere teleconnection patterns during extreme phases of zonal-mean circulation. *J. Climate*, **9**, 2614-2633.

- Uppala, S. M., and Coauthors, 2005: The ERA-40 re-analysis. *Quart. J. Roy. Meteor. Soc.*, **131**, 2961-3012.
- von Storch, H., and F. W. Zwiers, 1999: *Statistical Analysis in Climate Research*. Cambridge University Press, 484 pp.
- Wittman, M. A. H., L. M. Polvani, R. K. Scott, and A. J. Charlton, 2004: Stratospheric influence on baroclinic lifecycles and its connection to the Arctic oscillation. *Geophys. Res. Lett.*, **31**, L16113, doi:10.1029/2004GL020503.
- Wittman, M. A. H., A. J. Charlton, and L. M. Polvani, 2007: The effect of lower stratospheric shear on baroclinic instability. *J. Atmos. Sci.*, **64**, 479-496.

List of Figures

Figure 1. Cross-spectral analysis between the NAM index at 20 hPa and the vertical EP flux anomalies averaged over 45°-75°N at (a, b) 100 hPa, (c, d) 500 hPa. Dashed and thin solid lines are the 95% and 99% confidence levels respectively. The NCEP-NCAR reanalysis.

Figure 2. Cross-spectral analysis between the NAM index at 20 hPa and 70 hPa. Dashed and thin solid lines are the 95% and 99% confidence levels respectively. The NCEP-NCAR reanalysis.

Figure 3. Correlation between the December-January NAM index at 20 hPa and (top) the November-December, (bottom) the January-February vertical EP flux anomalies. The (left) NCEP-NCAR reanalysis and the (right) LMDz GCM. Positive contour values are solid, negative values are dotted and zero contours are dashed. The thick black line is the tropopause for respective periods. The 5% (lines) and 1% (solid) significance levels are shaded (two-side *t* test).

Figure 4. Cross correlation of the 60-day low-passed NAM index at 20 hPa with itself and with the 60-day low-passed vertical EP flux anomalies averaged over 45°-75°N. The (top two plots) NCEP-NCAR reanalysis and the (bottom two plots) LMDz GCM. Contours and shading as in Fig. 3.

Figure 5. Cross correlation of the 60-day low-passed NAM index at 20 hPa with the 60-day low-passed vertical EP flux anomalies. Cross-correlations are taken at lags a) -25, b) -10, c) 10 and, d) 25 days. Contours and shading as in Fig. 3. The NCEP-NCAR reanalysis.

Figure 6. Cross correlation of the 60-day low-passed NAM index at 20 hPa with the 60-day low-passed vertical EP flux anomalies taken at (solid) 100 hPa over 45°-75°N, (dotted) 400 hPa over 45°-75°N and, (dashed) at 400 hPa, 70°N. Dashed-dotted line is the 1% significance level. The NCEP-NCAR reanalysis.

Figure 7. Cross correlation of the 60-day low-passed NAM index at 20 hPa with the 60-day low-passed anomalies of (a) zonal mean zonal wind and (b) zonal mean zonal wind shear at lag 10 days. Contours and shading as in Fig. 3. The NCEP-NCAR reanalysis.

Table 1. Minimum and maximum cross correlation between the 60-day low-passed 20-hPa NAM index and the 60-day low-passed vertical EP flux anomalies (1979-2005), lag in days, and p -values for the one-side paired difference permutation test with the null hypothesis

$$H_0 : |\overline{\mathbf{R}_{\max}}| - |\overline{\mathbf{R}_{\min}}| \leq 0.$$

EP flux	\mathbf{R}_{\min} (lag)	\mathbf{R}_{\max} (lag)	p -value
45°-75°N, 100 hPa	-0.7 (-19)	0.62 (25)	0.965
45°-75°N, 400 hPa	-0.3 (-33)	0.51 (16)	0.001
70°N, 400 hPa	-0.33 (-40)	0.61 (11)	< 0.001

NCEP-NCAR

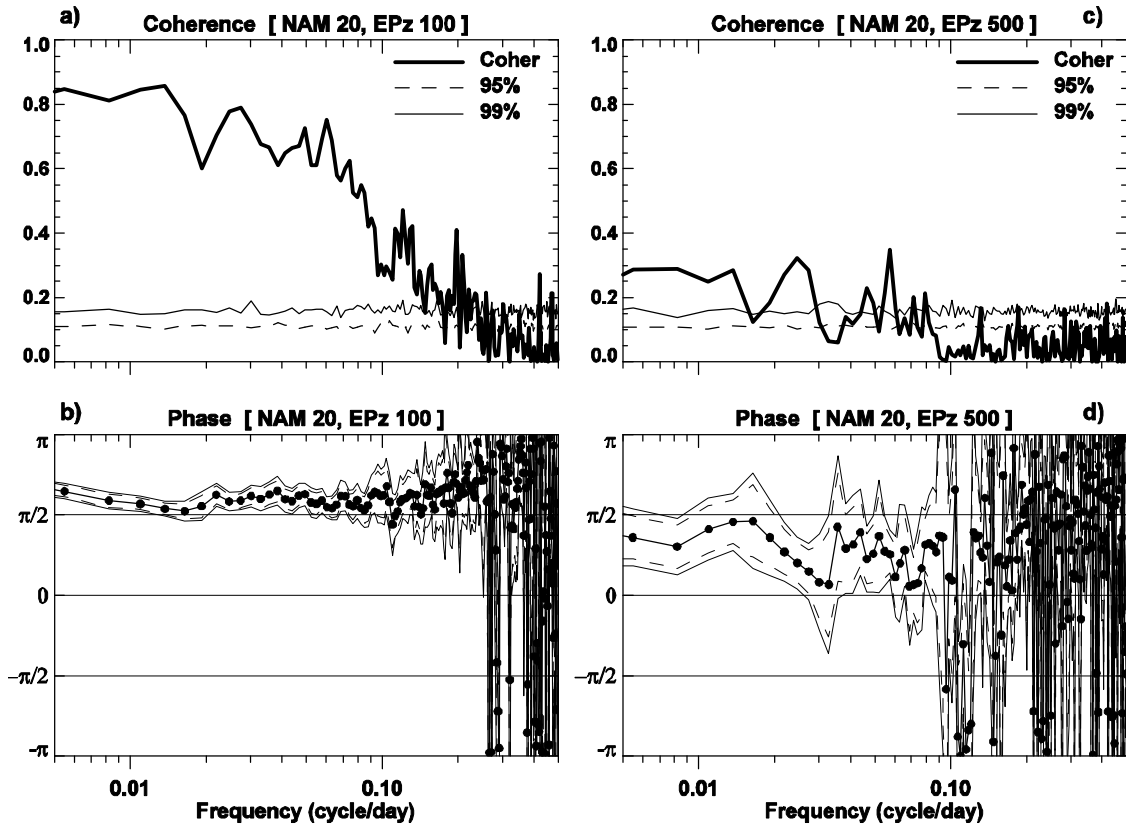


Figure 1. Cross-spectral analysis between the NAM index at 20 hPa and the vertical EP flux anomalies averaged over 45° - 75° N at (a, b) 100 hPa, (c, d) 500 hPa. Dashed and thin solid lines are the 95% and 99% confidence levels respectively. The NCEP-NCAR reanalysis.

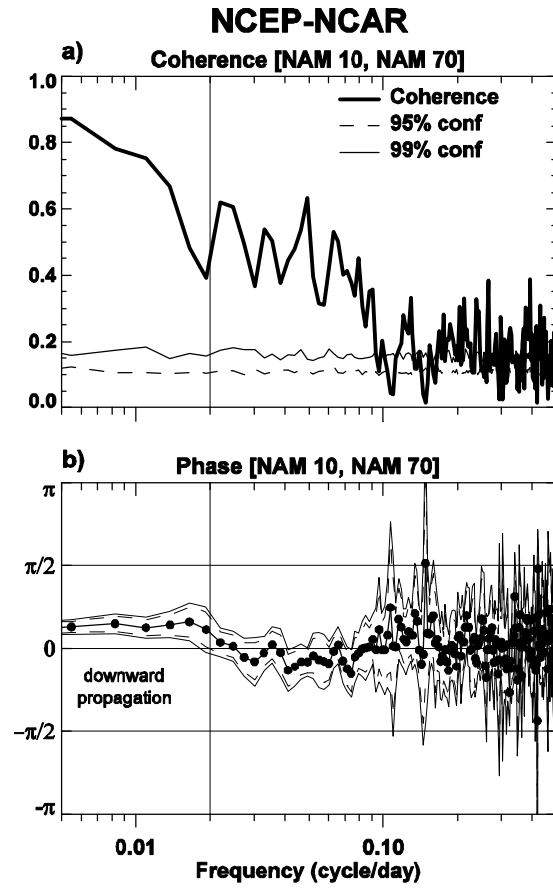


Figure 2. Cross-spectral analysis between the NAM index at 20 hPa and 70 hPa. Dashed and thin solid lines are the 95% and 99% confidence levels respectively. The NCEP-NCAR reanalysis.

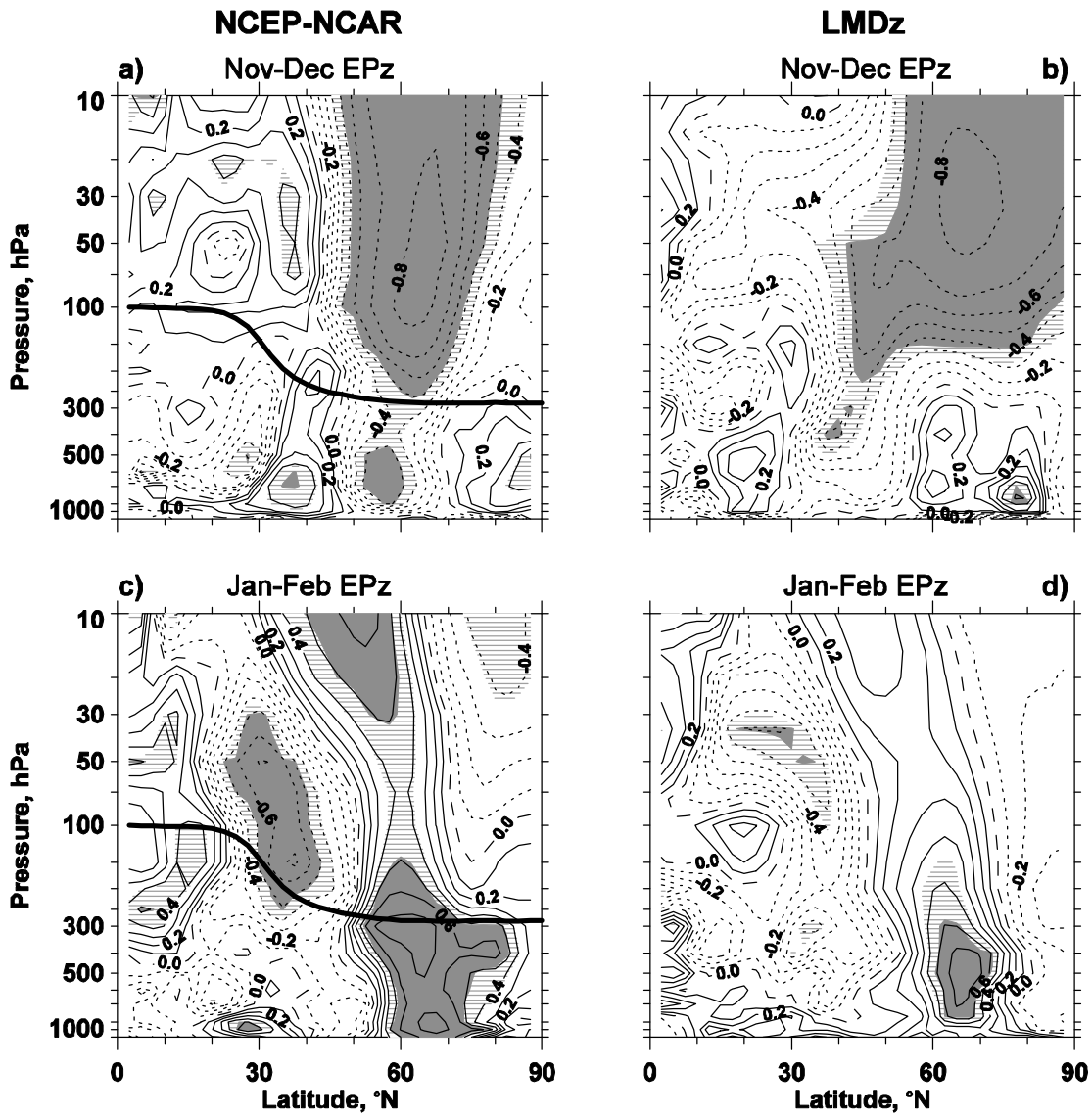


Figure 3. Correlation between the December-January NAM index at 20 hPa and (top) the November-December, (bottom) the January-February vertical EP flux anomalies. The (left) NCEP-NCAR reanalysis and the (right) LMDz GCM. Positive contour values are solid, negative values are dotted and zero contours are dashed. The thick black line is the tropopause for respective periods. The 5% (lines) and 1% (solid) significance levels are shaded (two-side t test).

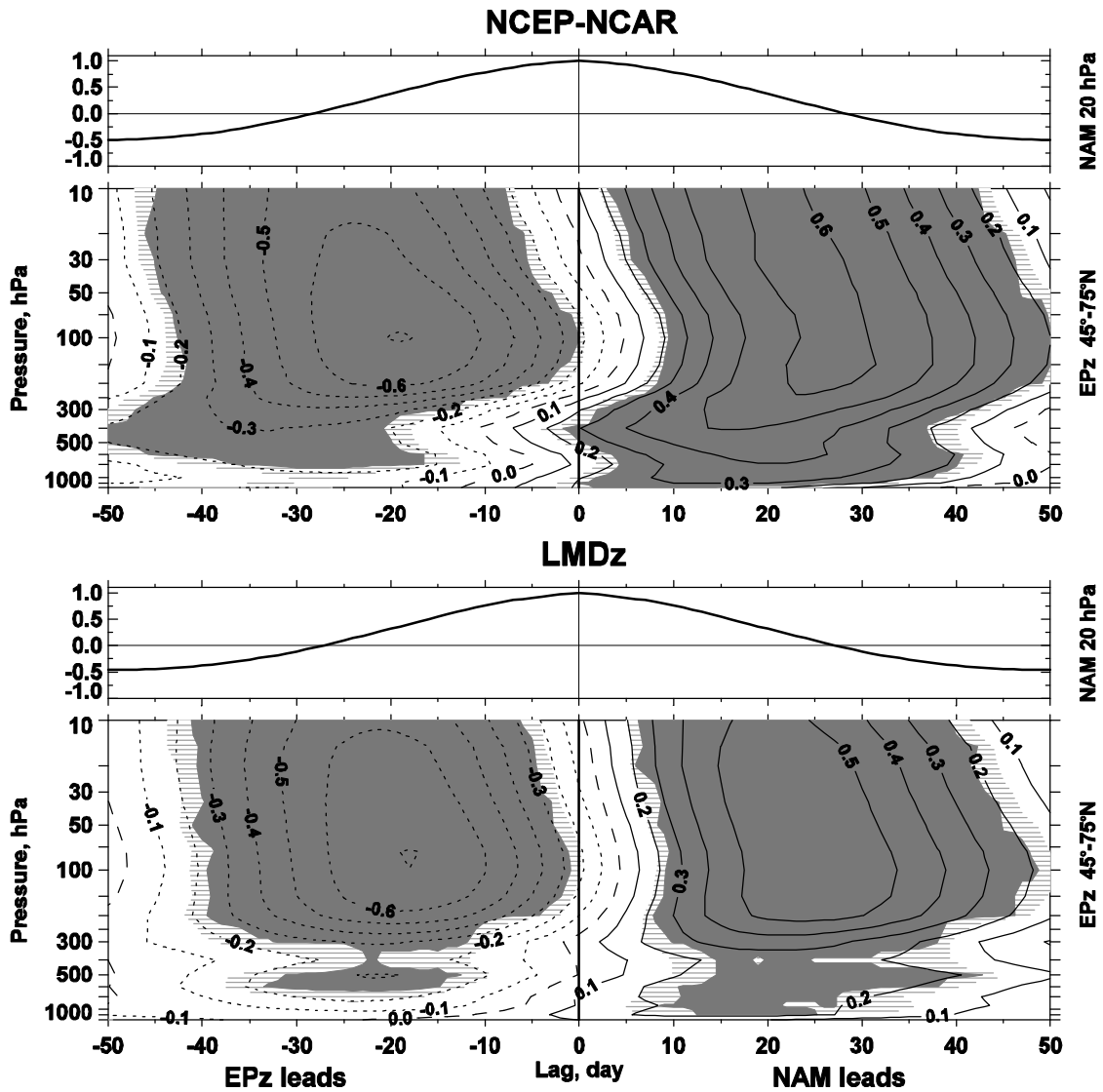


Figure 4. Cross correlation of the 60-day low-passed NAM index at 20 hPa with itself and with the 60-day low-passed vertical EP flux anomalies averaged over 45°-75°N. The (top two plots) NCEP-NCAR reanalysis and the (bottom two plots) LMDz GCM. Contours and shading as in Fig. 3.

NCEP-NCAR

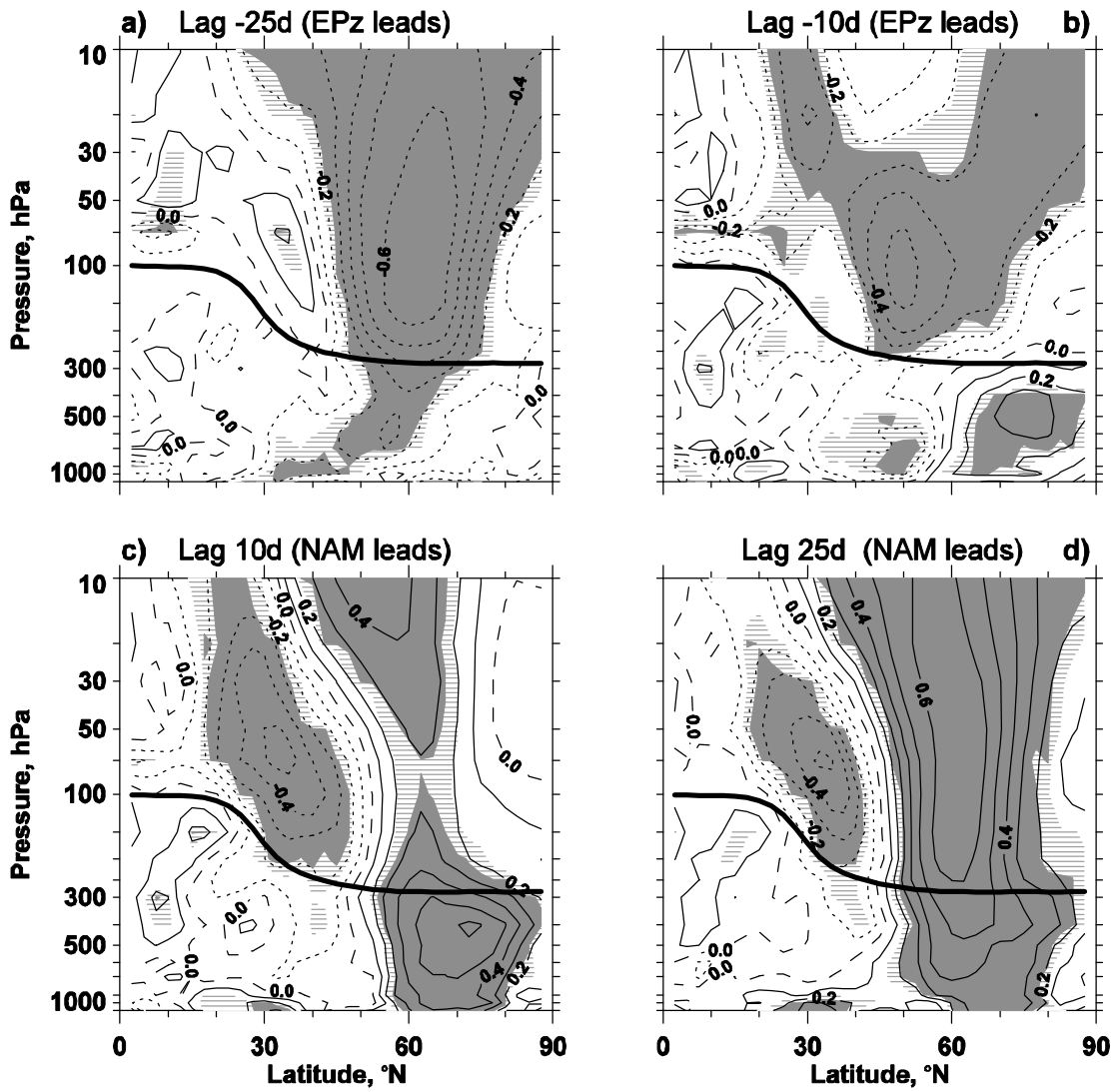


Figure 5. Cross correlation of the 60-day low-passed NAM index at 20 hPa with the 60-day low-passed vertical EP flux anomalies. Cross-correlations are taken at lags a) -25, b) -10, c) 10 and, d) 25 days. Contours and shading as in Fig. 3. The NCEP-NCAR reanalysis.

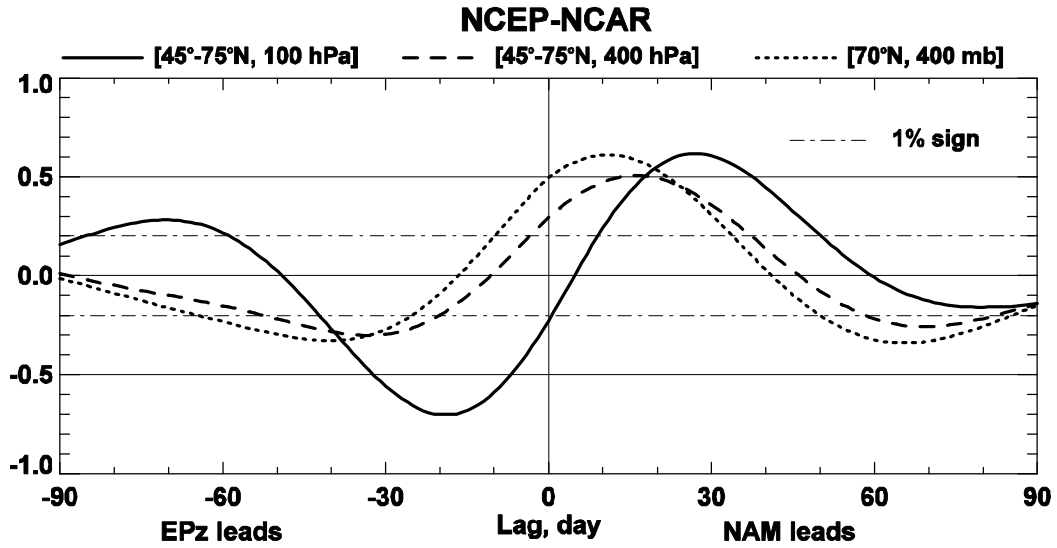


Figure 6. Cross correlation of the 60-day low-passed NAM index at 20 hPa with the 60-day low-passed vertical EP flux anomalies taken at (solid) 100 hPa over 45°-75°N, (dotted) 400 hPa over 45°-75°N and, (dashed) at 400 hPa, 70°N. Dashed-dotted line is the 1% significance level. The NCEP-NCAR reanalysis.

NCEP-NCAR

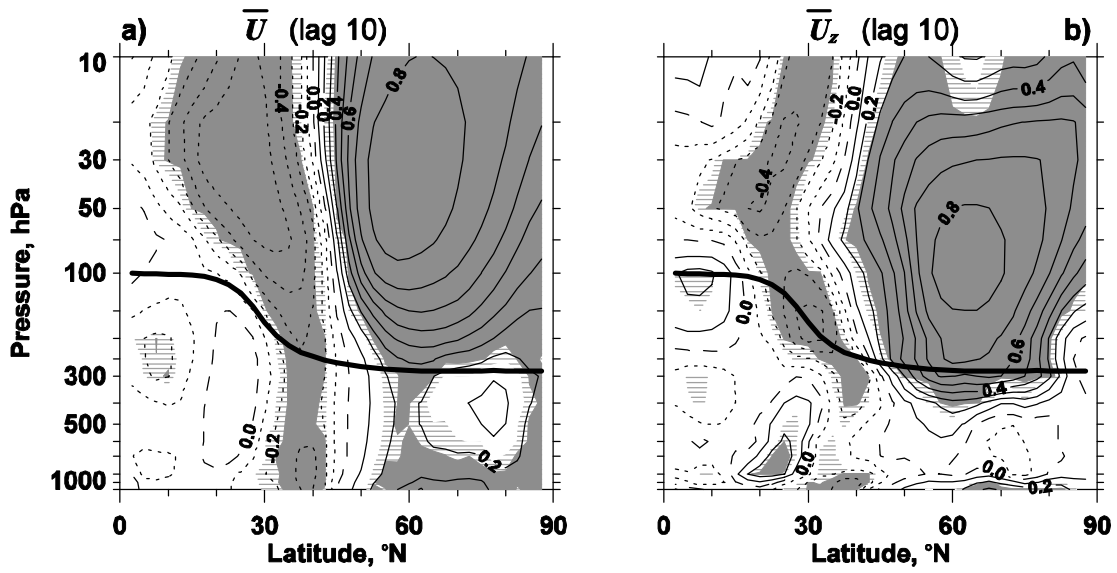


Figure 7. Cross correlation of the 60-day low-passed NAM index at 20 hPa with the 60-day low-passed anomalies of (a) zonal mean zonal wind and (b) zonal mean zonal wind shear at lag 10 days. Contours and shading as in Fig. 3. The NCEP-NCAR reanalysis.